CENTRE FOR **STOCHASTIC GEOMETRY**
AND ADVANCED **BIOIMAGING**

Johanna F. Ziegel, Jens R. Nyengaard and Eva B. Vedel Jensen

Applied tensor stereology

No. 10, May 2014

Applied tensor stereology

Johanna F. Ziegel[1], Jens R. Nyengaard[2] and Eva B. Vedel Jensen[3]

[1]Department of Mathematics and Statistics, University of Bern,
johanna.ziegel@stat.unibe.ch
[2]Stereology and EM Laboratory, Clinical Institute, Aarhus University,
nyengaard@ki.au.dk
[3]Department of Mathematics, Aarhus University, eva@imf.au.dk

Abstract

In the present paper, statistical procedures for estimating shape and orientation of arbitrary three-dimensional particles are developed. The focus of this work is on the case where the particles cannot be observed directly, but only via sections. Volume tensors are used for describing particle shape and orientation, and stereological estimators of the tensors are derived. It is shown that these estimators can be combined to provide consistent estimators of the moments of the so-called particle cover density. The covariance structure associated with the particle cover density depends on the orientation and shape of the particles. For instance, if the distribution of the typical particle is invariant under all rotations, then the covariance matrix is proportional to the identity matrix. A non-parametric test for such isotropy is developed. A flexible Lévy-based particle model is proposed, which may be analysed using a generalized methods of moments in which the volume tensors enter. The developed methods are used to study the cell organization in the human brain cortex.

Keywords: Ellipsoidal approximation, Local stereology, Optical rotator, Particle cover density, Particle shape, Particle orientation, Volume tensors

1 Introduction

Inference about shape and orientation of particles plays a fundamental role in the analysis of data, obtained by a wide range of imaging techniques. In cases where it is impossible to observe the particles directly, it is challenging to obtain valid shape and orientation information without initially restricting to a subclass of shapes. In such cases, the particles may only be observable in sections or through projections. Early examples where shape analysis was done under restrictions to small classes of shapes may be found in Cruz-Orive (1976, 1978) where ellipsoidal particles were analysed using random sections.

In the present paper, we take up this problem. We associate to each (arbitrarily shaped) particle a collection of volume tensors. These tensors are used as descriptors

of particle size, position, shape and orientation. The volume tensor of rank 0 is simply the volume of the particle while a normalized version of the volume tensor of rank 1 is the centre of gravity of the particle. The volume tensor of rank 2 contains information about particle shape and orientation.

If a 3D voxel image of each sampled particle can be constructed by the imaging technique in question, it is fairly straightforward to determine the volume tensors precisely and make inference by standard statistical techniques. For instance, for volume tensors of rank 2, the approach yields a sample of 3×3 positive definite matrices. Such analyses of volume tensors, or more generally Minkowski tensors, have been used with success for shape description in material science (Beisbart et al., 2002; Denis et al., 2008; Schröder-Turk et al., 2011a,b), and there are also examples from the biosciences (Beisbart et al., 2006).

In the present paper, we focus on the more difficult situation where the construction of such 3D voxel images is not feasible. Even in conventional microscopy, it is difficult to construct such images. For this case, we develop stereological methods of estimating volume tensors. The main practical purpose of stereology is to estimate quantitative parameters of a spatial object from microscopy images of sections through the object (Baddeley and Jensen, 2005). A recent account of the mathematical and statistical foundations of stereology and the closely related field of stochastic geometry can be found in Schneider and Weil (2008). Local stereology is concerned with estimators based on observations in sections through fixed lower dimensional subspaces (Jensen, 1998).

Local stereology of volume tensors (and more generally Minkowski tensors) has been studied in the recent papers by Auneau-Cognacq et al. (2013) and Jensen and Ziegel (2013). In Jensen and Ziegel (2013), the focus is on local stereological estimation, using lines and planes passing through fixed points. In the present paper, we show how a number of other geometric designs can be used for estimating volume tensors, including the Cavalieri design and the optical rotator design (Baddeley and Jensen, 2005; Tandrup et al., 1997).

If the estimator variances are large, we cannot use these estimators in a direct study of the distribution of volume tensors of the particle population. We will show that the estimators can then instead be combined to provide consistent (in a probabilistic sense) estimators of moments of the so-called *particle cover density*. If we let $\mathbf{K}_0$ be a typical particle with reference point at the origin, the cover density takes the form

$$f_{\mathbf{K}_0}(x) = P(x \in \mathbf{K}_0)/\mathbb{E}V(\mathbf{K}_0), \quad x \in \mathbb{R}^3,$$

where V denotes volume. The density $f_{\mathbf{K}_0}$ may be envisaged as a kind of probability cloud, indicating how often the different points in space are visited by the typical particle $\mathbf{K}_0$. The covariance matrix of the cover density can be visualized by a centred ellipsoid called the *Miles ellipsoid*, containing information about average particle shape and orientation. We develop a non-parametric test of the hypothesis that the distribution of $\mathbf{K}_0$ is rotation invariant in which case the Miles ellipsoid is a ball.

An alternative to the non-parametric approach is to use a flexible stochastic particle model. Such a model, defined as a kernel smoothing of a Lévy basis, is also developed in the paper extending the approach of Hansen et al. (2011). The mean

values of the volume tensors are derived in terms of the model parameters which may be estimated, using a generalized method of moments. The model accommodates anisotropic particle distributions, in contrast to Hobolth (2003); Hannila et al. (2004). The particle model is used in a simulation study of the distribution of the non-parametric test for isotropy. More specifically, it is investigated how many particles have to be to sampled before the asymptotic distribution is a valid approximation to the exact distribution of the test statistic under consideration.

The paper is organized as follows. In Section 2, volume tensors are defined. Section 3 presents stereological designs by means of which volume tensors may be estimated from sections. In Section 4, the particle process is introduced as a marked point process, and estimators of moments of the cover density and their precision are derived as well as a non-parametric test for isotropy. The developed methods are used in Section 5 for the analysis of a data set obtained by optical microscopy of the human brain cortex. In Section 6, the Lévy-based stochastic particle model is defined and subsequently used in a parametric analysis of the data. A simulation study of the performance of the developed statistical procedures is presented in Section 7. Technical details are deferred to two appendices.

2 Volume tensors

Let K be a compact subset of $\mathbb{R}^3$. We can associate to K a collection of volume tensors. The volume tensor of rank r is given by

$$\Phi_r(K) = \frac{1}{r!} \int_K x^r \, \mathrm{d}x, \quad r = 0, 1, \ldots \tag{2.1}$$

Here, x^r is the symmetric tensor of rank r determined by $x = (x_1, x_2, x_3)$. For $r = 0$ and 1, we have $x^0 = 1$ and $x^1 = x$, respectively. For $r = 2$, x^2 is a symmetric 3×3 matrix with entries

$$(x^2)_{i,j} = x_i x_j, \quad i, j = 1, 2, 3.$$

For general r, x^r can be represented as an $r-$dimensional array. The integration in (2.1) is to be understood coordinate-wise.

The volume tensors provide important information about the size, shape and orientation of K. The volume tensor of rank 0 is simply the volume of K, $\Phi_0(K) = V(K)$, while a normalized version of the volume tensor of rank 1 is the centre of gravity of K, $\Phi_1(K)/\Phi_0(K) = c(K)$. The volume tensor of rank 2 contains additional information about the shape and orientation of K.

To see this, let

$$\bar{K} = [K - c(K)]/V(K)^{1/3}$$

be a centred and rescaled version of K with unit volume. The volume tensor of rank 2 of $\bar{K}$ takes the form

$$\Phi_2(\bar{K}) = \frac{1}{\Phi_0(K)^{5/3}} \left(\Phi_2(K) - \frac{\Phi_1(K)^2}{2\Phi_0(K)} \right).$$

If K is an ellipsoid, then $\Phi_2(\bar{K})$ determines the directions and (up to a scale factor) the lengths of its semi-axes uniquely (Jensen and Ziegel, 2013). Thus, if

$$\Phi_2(\bar{K}) = B\Lambda B^* \tag{2.2}$$

is a spectral decomposition of $\Phi_2(\bar{K})$, then the columns of the orthogonal matrix B determine the directions of the semi-axes of K and the lengths of the semi-axes are

$$a_i = \left(\frac{3\,V(K)}{4\pi}\right)^{1/3} \frac{\lambda_i^{1/2}}{\prod_j \lambda_j^{1/6}}, \tag{2.3}$$

where λ_i, $i = 1, 2, 3$, are the diagonal elements of Λ.

For a general compact set K, we may still construct the spectral decomposition (2.2) of $\Phi_2(\bar{K})$. The centred ellipsoid with the same volume as K, directions of semi-axes given in the columns of B and lengths of semi-axes given by (2.3) will be denoted by $e(K)$. If K is actually an ellipsoid, then $K = c(K) + e(K)$. Otherwise, we may use $c(K) + e(K)$ as an ellipsoidal approximation to K, see Figure 1 for an illustration in 2D. Ellipsoidal approximations to a right circular cylinder and a rectangular parallelepiped are shown in Figure 2.

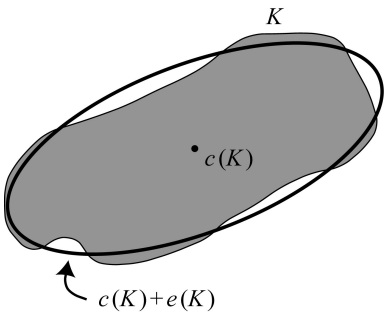

Figure 1: 2D illustration of the ellipsoidal approximation to a compact set K. Here, $c(K)$ is the centre of gravity and $e(K)$ is a centred ellipsoid, approximating $K - c(K)$. If K is an ellipsoid, then $K = c(K) + e(K)$.

Figure 2: Ellipsoidal approximations to a right circular cylinder and a rectangular parallelepiped in $\mathbb{R}^3$.

3 Stereological estimators of volume tensors

If K cannot be observed directly, but only via sections, we can estimate its volume tensors by stereological methods. In this section, we give examples of such stereological designs. The estimators are design-unbiased, that is unbiased with respect to the randomness of the design.

The Cavalieri design (Baddeley and Jensen, 2005, p. 155) uses a systematic set of planes with fixed orientation and uniform random position. The estimate of $\Phi_r(K)$ is given by

$$\widehat{\Phi}_r(K) = T \sum_i \frac{1}{r!} \int_{L_{2i}} \mathbf{1}\{x \in K\}\, x^r \mathrm{d}x,$$

where T is the distance between neighbour planes, the sum is taken over section planes and L_{2i} is the ith plane. If automatic segmentation of the planar section $K \cap L_{2i}$ is not available, $K \cap L_{2i}$ may be subsampled, using a uniformly placed point grid on $K \cap L_{2i}$. The resulting estimator takes the form

$$\widehat{\widehat{\Phi}}_r(K) = T \cdot a \sum_{ij} \frac{1}{r!} \mathbf{1}\{x_{ij} \in K\}\, x_{ij}^r,$$

where a is the area of the fundamental region of the point grid and x_{ij} is the jth point of the point grid on the ith section plane L_{2i}. Variance formulae for these estimators may be found in Baddeley and Jensen (2005, Chapter 13).

An alternative is to use local stereological estimators of $\Phi_r(K)$, based on measurements on random sections of K, passing through a reference point of K (Jensen and Ziegel, 2013). Such estimators have been constructed using a recently derived rotational Crofton formula (Auneau-Cognacq et al., 2013). Yet another possibility are estimators based on the intersection of K with a randomly rotating convex body $\mathbf{M}$ (Andersen et al., 2014).

The designs mentioned above require that the peripheral parts of K can be identified accurately. This is often not the case in optical microscopy, due to over-projection effects. A design that solves this problem is the optical rotator design that only uses measurements from the central part of K (Tandrup et al., 1997).

It turns out that this design can be used to estimate volume tensors. Thus, let L_2 be a plane passing through a centrally placed point in K, taken to be the origin O. Let $B(O,t)$ be the ball with centre at O and radius t. Then, $T_2 = L_2 + B(O,t)$ is a slice centred at O of thickness $2t$, see Figure 3.

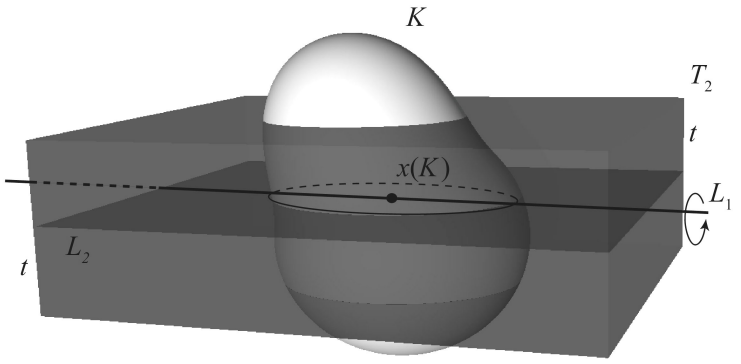

Figure 3: The optical rotator design by means of which $\Phi_r(K)$ may be estimated. The slice T_2 is randomly rotated around L_1.

We suppose that T_2 is a so-called vertical random slice, containing a fixed axis L_1 (the vertical axis), passing through O. Thus, T_2 is randomly rotated around L_1.

(In the data example to be presented later, T_2 is cut perpendicular to the brain surface.) Now, let $x \in \mathbb{R}^3$ be a fixed point in space. If we let $d(x, L_1)$ be the distance of x to L_1, then the probability that T_2 hits x is

$$P(x \in T_2) = \frac{2}{\pi} \arcsin(t/d(x, L_1)),$$

if $t \leq d(x, L_1)$, and 1, otherwise.

Using this result, we can construct a design-unbiased estimator of $\Phi_r(K)$ based on observations in the vertical random slice T_2,

$$\widehat{\Phi}_r(K) = \frac{1}{r!} \int_{K \cap T_2} x^r P(x \in T_2)^{-1} \, \mathrm{d}x.$$

More details are given in Appendix A where also procedures for subsampling of the slice with planes and subsequent subsampling of the planes with lines are described.

4 Inference for particle processes

We assume that the particle process X can be represented as a stationary marked point process. We thus assume that a reference point $x(K) \in K$ is associated to each particle $K \in X$, see Figure 4. The marked point process is then given by

$$\{[x(K); K - x(K)] : K \in X\}.$$

The particle (mark) distribution is denoted by $\mathbb{Q}$. We let $\mathbf{K}_0$ be a random compact set with distribution $\mathbb{Q}$. Here, $\mathbf{K}_0$ may be imagined as a randomly chosen particle or a typical particle with the origin O put at its reference point.

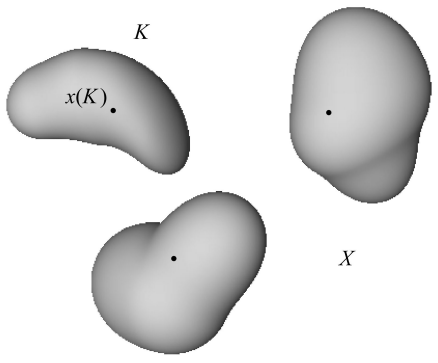

Figure 4: The particle process X is represented as a stationary marked point process in $\mathbb{R}^3$. A reference point $x(K) \in K$ is associated to each particle.

4.1 Sampling of particles

Let $\{K \in X : x(K) \in W\}$ be a sample of particles, where the Borel set $W \subseteq \mathbb{R}^3$ is a sampling window with $0 < V(W) < \infty$. (In Figure 5, it is illustrated how such a

3D sample of particles may be obtained, using optical microscopy.) The distribution of the tensors $\Phi_r(\mathbf{K}_0)$ of the typical particle $\mathbf{K}_0$ may be studied via the empirical distribution of

$$\{\Phi_r(K - x(K)) : K \in X, x(K) \in W\}. \tag{4.1}$$

This requires that, for each of the sampled particles, a 3D voxel image with satisfactory resolution is available.

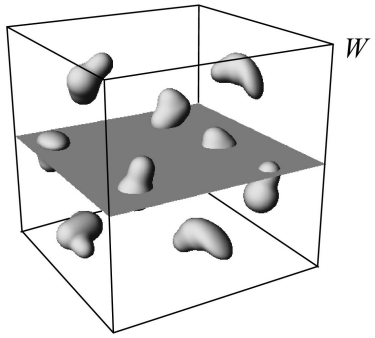

Figure 5: Sampling of particles K for which $x(K) \in W$. In optical microscopy, W is generated by moving the focal plane (shown dark grey) down through a transparent histological slab.

If complete access to the sampled particles is not possible, the distribution of $\Phi_r(\mathbf{K}_0)$ may still be studied via (4.1) if a precise estimate $\widehat{\Phi}_r(K - x(K))$ of $\Phi_r(K - x(K))$ is available. However, in the applications considered in this paper, the estimators of volume tensors have large variances and cannot be used directly in the study of the distribution of volume tensors in the particle population. Through a combination of a model- and design-based approach, the estimators may instead be used to provide consistent estimators of moments of the so-called *particle cover density*.

4.2 The particle cover density

The particle cover density is the probability density on $\mathbb{R}^3$ given by

$$f_{\mathbf{K}_0}(x) = P(x \in \mathbf{K}_0)/\mathbb{E}V(\mathbf{K}_0), \quad x \in \mathbb{R}^3.$$

The density $f_{\mathbf{K}_0}$ indicates how likely it is for a point in space to be visited by the typical particle $\mathbf{K}_0$.

Example 4.1. Suppose that the particle process consists of balls with their centres as reference points. Their radii are 1 or 2 with probability 1/2, cf. Figure 6, left. Then,

$$P(x \in \mathbf{K}_0) = \begin{cases} 1 & \text{if } \|x\| \leq 1, \\ \frac{1}{2} & \text{if } 1 < \|x\| \leq 2, \\ 0 & \text{if } \|x\| > 2. \end{cases}$$

Example 4.2. Suppose that the particle process consists of balls with radii 1, whose reference points are independent displacements of their centres following a normal

distribution with covariance $\sigma^2 I_3$, cf. Figure 6, right. Then, if we let $B(x, r)$ be the ball centred at $x \in \mathbb{R}^3$ and with radius r,

$$P(x \in \mathbf{K}_0) = \int_{B(x,1)} \varphi(u; \sigma^2)\, \mathrm{d}u,$$

where $\varphi(\cdot; \sigma^2)$ is the density of a normal distribution with covariance $\sigma^2 I_3$.

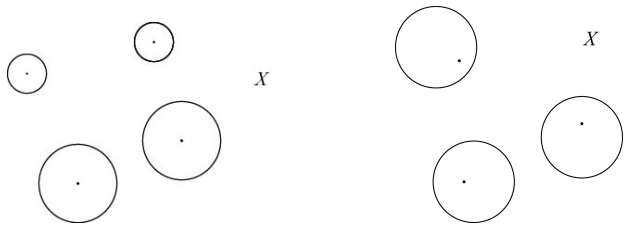

Figure 6: Two simple examples of particle processes.

If $\mathbf{K}_0$ is deterministic, then

$$f_{\mathbf{K}_0}(x) \propto \mathbf{1}(x \in \mathbf{K}_0),$$

and $\mathbf{K}_0$ can be reconstructed from $f_{\mathbf{K}_0}$. If $\mathbb{Q}$ is invariant under rotations, then $f_{\mathbf{K}_0}$ is also rotation invariant and $f_{\mathbf{K}_0}(x)$ only depends on the norm of x. If $\mathbb{Q}$ is invariant under rotations around an axis, represented by a line L_1 passing through O, then $f_{\mathbf{K}_0}(x)$ only depends on the distance of x to L_1. The last type of invariance will be called *restricted isotropy*.

Let $\mathbf{Y} \in \mathbb{R}^3$ be a random vector with density $f_{\mathbf{K}_0}$. Then, the mean of $\mathbf{Y}$ is

$$\mu = \mathbb{E}\mathbf{Y} = \int_{\mathbb{R}^3} x f_{\mathbf{K}_0}(x) \mathrm{d}x,$$

while the covariance matrix of $\mathbf{Y}$ is given by

$$\Sigma = \mathrm{Cov}(\mathbf{Y}) = \int_{\mathbb{R}^3} x^2 f_{\mathbf{K}_0}(x) \mathrm{d}x - \left(\int_{\mathbb{R}^3} x f_{\mathbf{K}_0}(x) \mathrm{d}x \right)^2.$$

Note that if $\mathbb{Q}$ is invariant under all rotations, then

$$\Sigma = \sigma^2 I_3,$$

while in the case where $\mathbb{Q}$ is invariant under rotations around L_1, then the spectral decomposition of Σ takes the form

$$\Sigma = B \tilde{\Lambda} B^T,$$

where the first column in the orthogonal matrix B is a unit vector, spanning L_1, and $\tilde{\Lambda} = \mathrm{diag}(\eta_1, \eta_2, \eta_3)$ with $\eta_2 = \eta_3$.

We may visualize Σ by the centred ellipsoid $e(X)$ which is uniquely determined by the equations $V(e(X)) = \mathbb{E}V(\mathbf{K}_0)$ and

$$\int_{e(X)} x^2 \frac{\mathrm{d}x}{V(e(X))} = \Sigma.$$

Notice that when $\mathbf{K}_0$ is deterministic, then $e(X) = e(\mathbf{K}_0)$. Furthermore, if all particles are translates of the same K, then $e(X) = e(K)$. We will call $e(X)$ the *Miles ellipsoid* of the particle process.

4.3 Estimation of moments of the cover density

The volume tensors of the particles are closely related to the cover density. In fact, the rth moment of the cover density is proportional to the mean particle volume tensor of rank r

$$\frac{\mathbb{E}\Phi_r(\mathbf{K}_0)}{\mathbb{E}V(\mathbf{K}_0)} = \frac{1}{r!}\int_{\mathbb{R}^3} x^r f_{\mathbf{K}_0}(x)\mathrm{d}x. \tag{4.2}$$

If precise estimation on the particle level is not possible, we may still get accurate information about the moments of the cover density. Let us suppose that $\widehat{\Phi}_r(K - x(K))$ is a design-unbiased estimator such that

$$\mathbb{E}(\widehat{\Phi}_r(K - x(K))|X) = \Phi_r(K - x(K)).$$

Let $K_1, \ldots, K_n$ be the sampled particles and let

$$Y_r = \frac{1}{n}\sum_{l=1}^{n} \widehat{\Phi}_r(K_l - x(K_l)), \quad r = 0, 1, 2.$$

Then, using (4.2),

$$\frac{\mathbb{E}Y_r}{\mathbb{E}Y_0} = \frac{1}{r!}\int_{\mathbb{R}^3} x^r f_{\mathbf{K}_0}(x)\mathrm{d}x. \tag{4.3}$$

The mean and covariance matrix of the cover density can be expressed as

$$\mu = \frac{\mathbb{E}Y_1}{\mathbb{E}Y_0}, \quad \Sigma = \frac{2\mathbb{E}Y_2}{\mathbb{E}Y_0} - \left(\frac{\mathbb{E}Y_1}{\mathbb{E}Y_0}\right)^2.$$

Therefore, the moments of the cover density can be estimated consistently, also in the case where the design variance $\mathrm{Var}(\widehat{\Phi}_r(K - x(K))|X)$ of $\widehat{\Phi}_r(K - x(K))$ is large. If the particles are i.i.d. this is clear from standard asymptotic theory. However, consistency also follows under much weaker assumptions on the particle process in an expanding window regime. For the case of a ergodic particle process, see Daley and Vere-Jones (2008, Corollary 12.2.V).

For $r = 1$, let $Y_1 = (Y_{11}, Y_{12}, Y_{13})$ and, for $r = 2$,

$$Y_2 = (Y_{2ij})_{i,j=1,2,3},$$

say. Consistent estimators of the elements μ_i and σ_{ij} of μ and Σ, respectively, are then

$$\widehat{\mu}_i = \frac{Y_{1i}}{Y_0}, \quad \widehat{\sigma}_{ij} = \frac{2Y_{2ij}}{Y_0} - \frac{Y_{1i}Y_{1j}}{Y_0^2}. \tag{4.4}$$

Using a Taylor expansion of the function $f(x, y) = x/y$, we find

$$\begin{aligned}\mathrm{cov}(\widehat{\mu}_i, \widehat{\mu}_{i'}) \approx{}& \frac{\mathrm{cov}(Y_{1i}, Y_{1i'})}{(\mathbb{E}Y_0)^2} - \mathrm{cov}(Y_{1i}, Y_0)\frac{\mathbb{E}Y_{1i'}}{(\mathbb{E}Y_0)^3} \\ &- \mathrm{cov}(Y_{1i'}, Y_0)\frac{\mathbb{E}Y_{1i}}{(\mathbb{E}Y_0)^3} + \mathrm{var}(Y_0)\frac{\mathbb{E}Y_{1i}\mathbb{E}Y_{1i'}}{(\mathbb{E}Y_0)^4}.\end{aligned} \tag{4.5}$$

Likewise, using a Taylor expansion of the function

$$\begin{aligned} f(x,y,z,v) &= \frac{2x}{y} - \frac{zv}{y^2} \\ &\approx f(x_0,y_0,z_0,v_0) + \frac{2}{y_0}(x-x_0) + \left(\frac{-2x_0}{y_0^2} + \frac{2z_0v_0}{y_0^3}\right)(y-y_0) \\ &\quad - \frac{v_0}{y_0^2}(z-z_0) - \frac{z_0}{y_0^2}(v-v_0), \end{aligned}$$

we find

$$\operatorname{cov}(\widehat{\sigma}_{ij}, \widehat{\sigma}_{i'j'}) \approx C_{ij;i'j'} + C_{i'j';ij}, \tag{4.6}$$

where

$$\begin{aligned} C_{ij;i'j'} &= \frac{2}{(\mathbb{E}Y_0)^6}\Delta_{ij}\Delta_{i'j'}\operatorname{var}Y_0 \\ &+ \frac{2\Delta_{ij}}{(\mathbb{E}Y_0)^5}\left[\mathbb{E}Y_{1j'}\operatorname{cov}(Y_0,Y_{1i'}) + \mathbb{E}Y_{1i'}\operatorname{cov}(Y_0,Y_{1j'})\right] - \frac{4}{(\mathbb{E}Y_0)^4}\Delta_{ij}\operatorname{cov}(Y_0,Y_{2i'j'}) \\ &+ \frac{1}{2(\mathbb{E}Y_0)^4}\left[\mathbb{E}Y_{1j}\mathbb{E}Y_{1j'}\operatorname{cov}(Y_{1i},Y_{1i'}) + 2\mathbb{E}Y_{1i}\mathbb{E}Y_{1j'}\operatorname{cov}(Y_{1j},Y_{1i'})\right. \\ &\qquad \left. + \mathbb{E}Y_{1i}\mathbb{E}Y_{1i'}\operatorname{cov}(Y_{1j},Y_{1j'})\right] \\ &- \frac{2}{(\mathbb{E}Y_0)^3}\left[\mathbb{E}Y_{1j}\operatorname{cov}(Y_{1i},Y_{2i'j'}) + \mathbb{E}Y_{1i}\operatorname{cov}(Y_{1j},Y_{2i'j'})\right] + \frac{2}{(\mathbb{E}Y_0)^2}\operatorname{cov}(Y_{2ij},Y_{2i'j'}), \end{aligned}$$

and

$$\Delta_{ij} = \mathbb{E}Y_{2ij}\mathbb{E}Y_0 - \mathbb{E}Y_{1i}\mathbb{E}Y_{1j}.$$

Note that the right-hand sides of (4.5) and (4.6) may be consistently estimated if the particles $K_1, \ldots, K_n$ are assumed to be i.i.d., or, in an expanding window regime, if the particle process is ergodic (Daley and Vere-Jones, 2008, Corollary 12.2.V).

4.4 Estimation of Σ under rotational invariance

The estimate $\widehat{\Sigma} = (\widehat{\sigma}_{ij})_{ij}$ of the covariance matrix Σ of the cover density, with $\widehat{\sigma}_{ij}$ given at (4.4), is generally applicable without assumptions about rotational invariance.

Under the isotropy model (invariance under all rotations), we have $\Sigma = \sigma^2 I_3$. We suggest to estimate σ^2 by $\widehat{\sigma^2}$ which is the minimizer β of the Frobenius matrix norm of

$$\widehat{\Sigma} - \beta I_3,$$

where

$$\widehat{\Sigma} = \frac{2Y_2}{Y_0} - \left(\frac{Y_1}{Y_0}\right)^2.$$

We obtain

$$\widehat{\sigma^2} = \arg\min_{\beta} \sqrt{\sum\nolimits_{i=1}^{3}(\hat{\eta}_i - \beta)^2} = \tfrac{1}{3}(\hat{\eta}_1 + \hat{\eta}_2 + \hat{\eta}_3),$$

where $\hat{\eta}_1, \hat{\eta}_2, \hat{\eta}_3$ are the eigenvalues of $\widehat{\Sigma}$.

Under the restricted isotropy model (invariance under rotations around an axis L_1), we have $\Sigma = B\tilde{\Lambda}B^T$, where the orthogonal matrix B is known and $\tilde{\Lambda} = \mathrm{diag}(\eta_1, \eta_2, \eta_3)$ with $\eta_2 = \eta_3$. We suggest to estimate η_1 and η_2 by minimizing the Frobenius matrix norm between the theoretical covariance matrix under restricted isotropy and $\widehat{\Sigma}$.

4.5 A non-parametric test for isotropy

In an actual application, it is clearly of interest to test the hypothesis that the distribution $\mathbb{Q}$ of $\mathbf{K}_0$ is rotation invariant. Under isotropy, the covariance matrix Σ of the cover density is proportional to the identity matrix. We thus want to test the following hypothesis

$$H_0 : \sigma_{ii} = \sigma^2 > 0, \sigma_{ij} = 0, i \neq j.$$

For convenience, let

$$Z = (Z_1, Z_2, Z_3, Z_4, Z_5, Z_6) = (\widehat{\sigma}_{11}, \widehat{\sigma}_{22}, \widehat{\sigma}_{33}, \widehat{\sigma}_{12}, \widehat{\sigma}_{13}, \widehat{\sigma}_{23}),$$

where $\widehat{\sigma}_{ij}$ is given at (4.4). We approximate the distribution of Z by a 6-dimensional normal distribution with mean

$$(\sigma_{11}, \sigma_{22}, \sigma_{33}, \sigma_{12}, \sigma_{13}, \sigma_{23})$$

and covariance matrix $\mathrm{cov}(Z) = \Lambda$. This approximation is justified by the delta method for reasonably large n.

The hypothesis H_0 can now be tested as follows. Let

$$\bar{Z}_{13} = (Z_1 + Z_2 + Z_3)/3.$$

Then, under H_0

$$U = (Z_1 - \bar{Z}_{13}, Z_2 - \bar{Z}_{13}, Z_4, Z_5, Z_6)$$

is approximately $N_5(0, A\Lambda A^T)$-distributed, where A is the 5×6 matrix with elements

$$a_{ij} = \begin{cases} \frac{2}{3}, & \text{if } i = j, i \in \{1, 2\}, \\ -\frac{1}{3}, & \text{if } i \neq j, i \in \{1, 2\}, j \in \{1, 2, 3\}, \\ 1, & \text{if } i = j - 1, i \in \{3, 4, 5\}, \\ 0, & \text{otherwise.} \end{cases}$$

As test statistic, we can use $T = U(A\Lambda A^T)^{-1}U^T$ which is approximately $\chi^2(5)$-distributed under H_0. Large values of T are critical for H_0. In an actual application of the test statistic T, Λ has to be replaced by an estimate.

An estimate of Λ may be derived by using the approximation (4.6) of the elements of Λ and replacing theoretical moments by empirical moments, obtained from measurements on n particles. The test statistic T shows the right level for smaller n if it is used that under the isotropy hypothesis

$$\mathbb{E}Y_2 = \left[\sigma^2 \mathbb{E}Y_0 \, I_3 + \frac{(\mathbb{E}Y_1)^2}{\mathbb{E}Y_0}\right]/2, \tag{4.7}$$

and $\mathbb{E}Y_2$ is replaced in (4.6) by the right-hand side of (4.7) in all the terms where it appears. In particular, we also replace $\mathbb{E}Y_2$ by the right-hand side of (4.7) in the terms of the form $\mathrm{cov}(Y_*, Y_{2ij}) = \mathbb{E}Y_*Y_{2ij} - \mathbb{E}Y_*\mathbb{E}Y_{2ij}$. Hence, the estimates $\widehat{\Phi}_2(K_l - x(K_l))$ are only used to estimated the mixed moments $\mathbb{E}Y_*Y_{2ij}$.

The statistical performance of the test is investigated in a simulation study, presented in Section 7, for the stochastic particle model presented in Section 6.

5 Data analysis – non-parametric inference

The data has been collected from one histological slab W of thickness 140 µm through the human brain cortex. The section has been taken perpendicular to the brain surface and with a random rotation around the normal to the brain surface. The focus in the investigation was on the pyramidal neurons that are known to be orientated perpendicular to the brain surface. The question to be examined in the investigation was whether the directional properties of the pyramidal neurons are reflected in an elongation of their nuclei in the same direction perpendicular to the brain surface.

A total of $n = 100$ neuron nuclei were measured. The nucleolus was used as reference point. For each sampled nucleus, the volume tensors of rank 0, 1 and 2 were estimated, using locally the optical sectioning design illustrated in Figure 3 with L_2 parallel to the surface of the big histological section. In all cases $t = 2.5$ µm. For each nucleus, the optical slice T_2 was subsampled by a systematic set of planes parallel to L_2 with distance 1.67 µm between neighbour planes and the planes were subsampled by a systematic set of lines that alternatingly was parallel to the vertical axis L_1 and perpendicular to L_1, see Appendix A. The distance was 5 µm between neighbour lines within a plane. It took about $2\frac{1}{2}$ hours to collect these measurements for all 100 nuclei.

For all nuclei (in the coordinate systems relative to their reference points), we have (approximately)

$$u = \begin{pmatrix} 0.987 \\ -0.162 \\ 0 \end{pmatrix}, \quad v = \begin{pmatrix} 0 \\ 0 \\ 1 \end{pmatrix}, \quad w = \begin{pmatrix} -0.162 \\ -0.987 \\ 0 \end{pmatrix}.$$

Here, u is spanning the direction perpendicular to the brain surface while v is perpendicular to the histological slab.

The estimated mean particle volume and estimated variance are

$$Y_0 = 606.535, \quad \mathrm{var}(Y_0) \approx \frac{1}{n} 57751.57 = 577.516.$$

Using the approximation formula (4.5) for the covariance matrix of $\widehat{\mu}$, we obtain

$$\widehat{\mu} = \begin{pmatrix} -0.111 \\ -0.224 \\ 0.069 \end{pmatrix}, \quad \mathrm{cov}(\widehat{\mu}) \approx \frac{1}{n} \begin{pmatrix} 1.5 & 0.391 & 0.073 \\ 0.391 & 3.34 & -0.157 \\ 0.073 & -0.157 & 0.404 \end{pmatrix}.$$

The estimated covariance $\widehat{\Sigma}$ of the cover density is

$$\widehat{\Sigma} = \begin{pmatrix} 9.479 & 0.575 & 0.04 \\ 0.575 & 11.274 & -0.058 \\ 0.04 & -0.058 & 1.992 \end{pmatrix}.$$

Using the approximation (4.6), the matrix of estimated variances $\mathrm{var}(\widehat{\Sigma}) = \{\mathrm{var}(\widehat{\sigma}_{ij})\}_{ij}$ becomes

$$\mathrm{var}(\widehat{\Sigma}) = \frac{1}{n}\begin{pmatrix} 13.505 & 11.778 & 1.125 \\ 11.778 & 37.851 & 1.867 \\ 1.125 & 1.867 & 0.37 \end{pmatrix}.$$

For the spectral decomposition of $\widehat{\Sigma} = BDB^\top$ we obtain

$$B = \begin{pmatrix} -0.281 & 0.96 & -0.006 \\ -0.96 & -0.281 & 0.007 \\ 0.005 & 0.007 & 1 \end{pmatrix}, \quad D = \begin{pmatrix} 11.443 & 0 & 0 \\ 0 & 9.311 & 0 \\ 0 & 0 & 1.992 \end{pmatrix}.$$

In the present application, we will use that the developed estimators of volume tensors can be used in a model-based setting with restricted isotropy without actually generating independently rotated optical slices for each sampled particle. This is a very important observation, since it is generally unfeasible in optical microscopy to generate a new rotation for each sampled particle. For the collected data, the same rotation was used for all particles. The result is a Miles ellipsoid that is invariant under rotations around the vertical axis. This was no restriction for the biologists, involved in the project, because they were interested in the distributional properties in relation to the vertical axis.

Under the assumption of isotropy, the Miles ellipsoid is a sphere with radius 5.251. Under the assumption of restricted isotropy, the Miles ellipsoid is a prolate ellipsoid with the axis of rotation in the direction of u and semi-axis length 5.866 in this direction. The other half-axes have length 4.968.

The non-parametric test for isotropy rejects at level 5% the null-hypothesis of an isotropic particle distribution. We conclude that the neuron nuclei have an anisotropic distribution. Under restricted isotropy, the nuclei show slight elongation in the direction u perpendicular to the brain surface. This is consistent with the fact that the human cerebral cortex is developed in an inside-out manner where mitotically dividing progenitor cells in the centre of the brain are migrating outward towards the brain surface to form the neocortex.

6 A stochastic particle model

6.1 Description of the model

We consider particles $\mathbf{K}_0$, that are star-shaped with respect to $c_0 \in \mathbb{R}^3$, hence they can be written as $\mathbf{K}_0 = c_0 + \mathbf{M}$ for some particle $\mathbf{M}$ that is star-shaped with respect to the origin. Let $R\colon \mathbb{S}^2 \to [0,\infty)$ denote the radial function of $\mathbf{M}$.

We assume the following multiplicative model for R

$$R(u) = M(u)\varepsilon(u), \quad u \in \mathbb{S}^2, \tag{6.1}$$

where M is the radial function of a fixed star-shaped set $\mathcal{E}$, and $\varepsilon > 0$ is an isotropic random field on $\mathbb{S}^2$. In this manuscript, we only consider the case where $\mathcal{E}$ is an

ellipsoid that is centred at the origin with semi-axes lengths a_1, a_2, a_3, and $\varepsilon > 0$ is the random field on $\mathbb{S}^2$ that is given by

$$\varepsilon(u) = \int_{\mathbb{S}^2} k(u,v) Z(\mathrm{d}v),$$

where Z is a Gamma Lévy basis with parameters $\kappa, \tau > 0$ and

$$k(u,v) = e^{\alpha \cos d(u,v)}$$

is the von Mises-Fisher kernel proposed by Hansen et al. (2011). It has a parameter $\alpha > 0$ and $d(u,v)$ denotes the great circle distance between u and v. The short terminology of a Lévy basis has been introduced in Barndorff-Nielsen and Schmiegel (2004), see also Hellmund et al. (2008) and Jónsdóttir et al. (2008).

6.2 Moments of the cover density

The field ε is isotropic. Therefore, its moments are constant over the sphere and we define

$$\mathbb{E}(\varepsilon(u)^k) =: \mu_k.$$

In Appendix B, the moments μ_k are derived in terms of the model parameters κ, τ, α. For the moments of the cover density of $\mathbf{K}_0$ we first calculate the volume tensors of $\mathbf{K}_0$. We obtain with $u(\theta,\phi) = (\sin\theta\cos\varphi, \sin\theta\sin\varphi, \cos\theta)$, $\theta \in [0,\pi)$, $\varphi \in [0, 2\pi)$,

$$\begin{aligned}\Phi_0(\mathbf{K}_0) &= \int_{c_0+\mathbf{M}} \lambda_3(\mathrm{d}x) = \int_{\mathbf{M}} \lambda_3(\mathrm{d}x) = \int_0^\pi \int_0^{2\pi} \int_0^{R(u(\theta,\varphi))} r^2 \sin\theta \,\mathrm{d}r \,\mathrm{d}\varphi \,\mathrm{d}\theta \\ &= \frac{1}{3} \int_0^\pi \int_0^{2\pi} M(u(\theta,\varphi))^3 \varepsilon(u(\theta,\varphi))^3 \sin\theta \,\mathrm{d}\varphi \,\mathrm{d}\theta.\end{aligned}$$

Therefore,

$$\mathbb{E}V(\mathbf{K_0}) = \mathbb{E}\big(\Phi_0(\mathbf{K}_0)\big) = \mu_3 \Phi_0(\mathcal{E}) = \mu_3 \frac{4\pi}{3} a_1 a_2 a_3. \tag{6.2}$$

Similar calculations show that

$$\mathbb{E}\big(\Phi_1(\mathbf{K}_0)\big) = \mu_3 \Phi_0(\mathcal{E}) c_0 = \mu_3 \frac{4\pi}{3} a_1 a_2 a_3 \, c_0,$$

and

$$\begin{aligned}\mathbb{E}\big(\Phi_2(\mathbf{K}_0)\big) &= \mu_5 \Phi_2(\mathcal{E}) + \tfrac{1}{2}\mu_3 \Phi_0(\mathcal{E}) c_0^2 \\ &= \mathbb{E}\big(\Phi_2(\mathbf{M})\big) + \frac{1}{2\mathbb{E}\big(\Phi_0(\mathbf{K}_0)\big)} \mathbb{E}\big(\Phi_1(\mathbf{K}_0)\big)^2,\end{aligned}$$

because $\mathbb{E}\big(\Phi_2(\mathbf{M})\big) = \mu_5 \Phi_2(\mathcal{E})$. Using (4.2), the first moment of the cover density $f_{\mathbf{K}_0}$ is given by

$$\mu = \frac{\mathbb{E}\big(\Phi_1(\mathbf{K}_0)\big)}{\mathbb{E}\big(\Phi_0(\mathbf{K}_0)\big)} = c_0.$$

Its covariance matrix is

$$\Sigma = 2\frac{\mathbb{E}\Phi_2(\mathbf{K}_0)}{\mathbb{E}\Phi_0(\mathbf{K}_0)} - \left(\frac{\mathbb{E}\Phi_1(\mathbf{K}_0)}{\mathbb{E}\Phi_0(\mathbf{K}_0)}\right)^2 = 2\frac{\mathbb{E}\Phi_2(\mathbf{M})}{\mathbb{E}\Phi_0(\mathbf{M})} = \frac{3\mu_5}{2\pi\mu_3 a_1 a_2 a_3}\Phi_2(\mathcal{E}).$$

The semi-axes lengths a_1, a_2, a_3 of $\mathcal{E}$ and the eigenvalues $\lambda_1, \lambda_2, \lambda_3$ of $\Phi_2(\mathcal{E})$ are connected by $\lambda_i = 2\pi a_1 a_2 a_3 a_i^2/15$, $i = 1, 2, 3$; see Jensen and Ziegel (2013). Therefore, the eigenvalues η_1, η_2, η_3 of Σ are connected to the semi-axes lengths of $\mathcal{E}$ by the relation

$$a_i = \sqrt{\frac{5\mu_3}{\mu_5}\eta_i}, \quad i = 1, 2, 3. \tag{6.3}$$

A short calculation shows that the Miles ellipsoid $e(X)$ of the process is the ellipsoid with semi-axes $\mu_3^{1/3} a_i$, $i = 1, 2, 3$, in the same directions as the semi-axes of $\mathcal{E}$. This ellipsoid has volume $\mathbb{E}V(\mathbf{K}_0)$.

6.3 Fitting the parameters

Suppose we are given, with the notation from Section 4.3, estimates Y_0 of $\mathbb{E}(\Phi_0(\mathbf{K}_0)) = \mathbb{E}(V(\mathbf{K}_0))$ and Y_1/Y_0 of the mean μ of the cover density. Let $\tilde{\Sigma}$ be an estimate of the covariance matrix Σ of the cover density under the hypothesis about isotropy considered. For instance, if no rotation invariance is assumed

$$\tilde{\Sigma} = \frac{2Y_2}{Y_0} - \left(\frac{Y_1}{Y_0}\right)^2.$$

Estimates $\tilde{\Sigma}$ of Σ under (restricted) isotropy are given in Section 4.4.

We fix the parameter $\alpha = 4$, as this choice appears to generate reasonable particle shapes. The model parameters to be estimated are then the semi-axes lengths and directions of $\mathcal{E}$, the centre c_0 and the parameters τ and κ of the Lévy basis. We estimate c_0 by $\widehat{c}_0 = Y_1/Y_0$. Combining (6.2) and (6.3), we find

$$\mathbb{E}V(\mathbf{K}_0) = \mu_3\frac{4\pi}{3}a_1 a_2 a_3 = \frac{\mu_3^{5/2}}{\mu_5^{3/2}}\frac{5^{3/2}4\pi}{3}\sqrt{\eta_1\eta_2\eta_3}. \tag{6.4}$$

Since the left-hand side of (6.4) and the eigenvalues η_i of Σ can be estimated, we can use (6.4) as one of the estimating equations for τ and κ. As a second equation, we simply use $\mu_3 = 1$, which guarantees that $\mathbb{E}V(\mathbf{K}_0) = V(\mathcal{E})$, cf. (6.2). It remains to estimate the semi-axes lengths and directions of $\mathcal{E}$. The directions of the semi-axes of $\mathcal{E}$ are chosen as the directions of the eigenvectors of $\tilde{\Sigma}$. The semi-axes lengths are obtained as a plug-in estimate using (6.3).

6.4 Data analysis - parametric inference

Using the generalized method of moments described in Section 6.3, we fit the parameters of the stochastic particle model to the particle data described in Section 5, under no rotational invariance, and under the assumptions of isotropy or restricted isotropy; see Section 4.4. The resulting parameter values are summarized in Tables 1 and 2, respectively.

Table 1: Parameters of the anisotropic model for $\mathbf{K}_0$. The parameters for $\mathcal{E}$ are the semi-axes' lengths and directions.

$\mathcal{E}$	$a = 7.273$, $(-0.281, -0.96, 0.005)^\top$ $b = 6.561$, $(0.96, -0.281, 0.007)^\top$ $c = 3.034$, $(-0.006, 0.007, 1)^\top$
c_0	$(-0.111, -0.224, 0.069)^\top$
τ	1740.415
κ	19.982

Table 2: Parameters of the isotropic and restricted isotropy model for $\mathbf{K}_0$. The parameters for $\mathcal{E}$ are the semi-axes' lengths and directions.

	Isotropic model	Restricted isotropy model
$\mathcal{E}$	$a = b = c = 5.251$	$a = 5.866$, $(0.987, -0.162, 0)^\top$ $b = c = 4.968$
c_0	$(-0.111, -0.224, 0.069)^\top$	$(-0.111, -0.224, 0.069)^\top$
τ	425.923	443.752
κ	4.652	4.860

As the hypothesis of an isotropic model is clearly rejected by the presented non-parametric test, we do not investigate this model. Furthermore, the data did not contain enough information to provide a reliable estimate of a tri-axial Miles ellipsoid in the anisotropic model, due to the reasons described at the end of Section 5. This was also confirmed by a visual comparison of simulated and observed particle profiles. The simulated profiles showed much less variability than the observed profiles. In contrast, the restricted isotropy model provides a satisfactory fit to the data, as judged from visual inspection of observed and simulated profiles. Figure 7 shows the profiles of the 100 measured particles in a plane through the reference point perpendicular to $v = (0, 0, 1)^\top$. For comparison, in Figure 8 simulated profiles under the restricted isotropy model are provided. The vertical axis u is shown as a drawn line for reference. Images of simulated 3D particles under restricted isotropy are given in Figure 9.

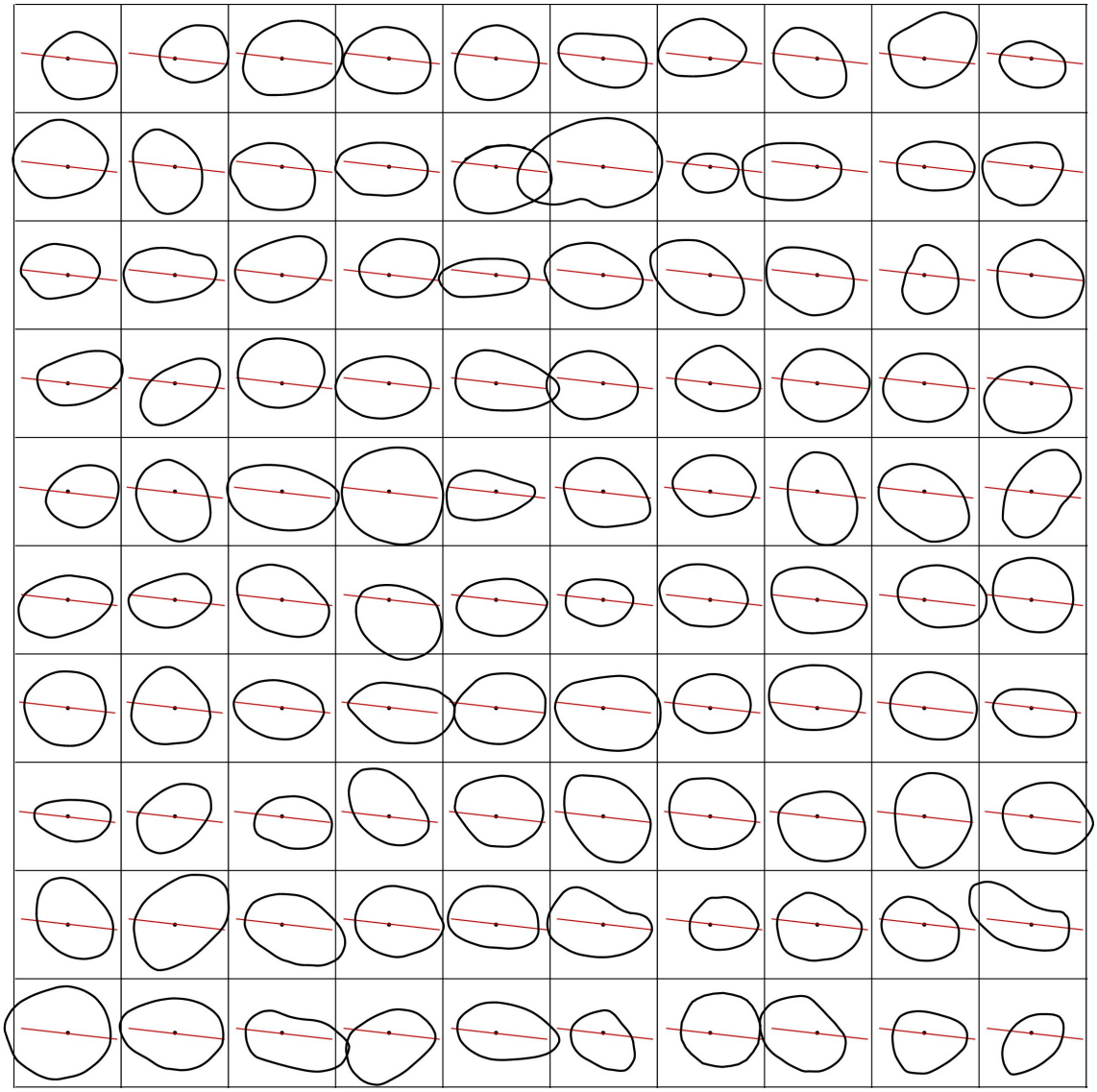

Figure 7: Profiles of the 100 measured particles in a plane through their reference points perpendicular to $v = (0, 0, 1)^\top$. The direction of the vertical axis u is marked as a line for each particle.

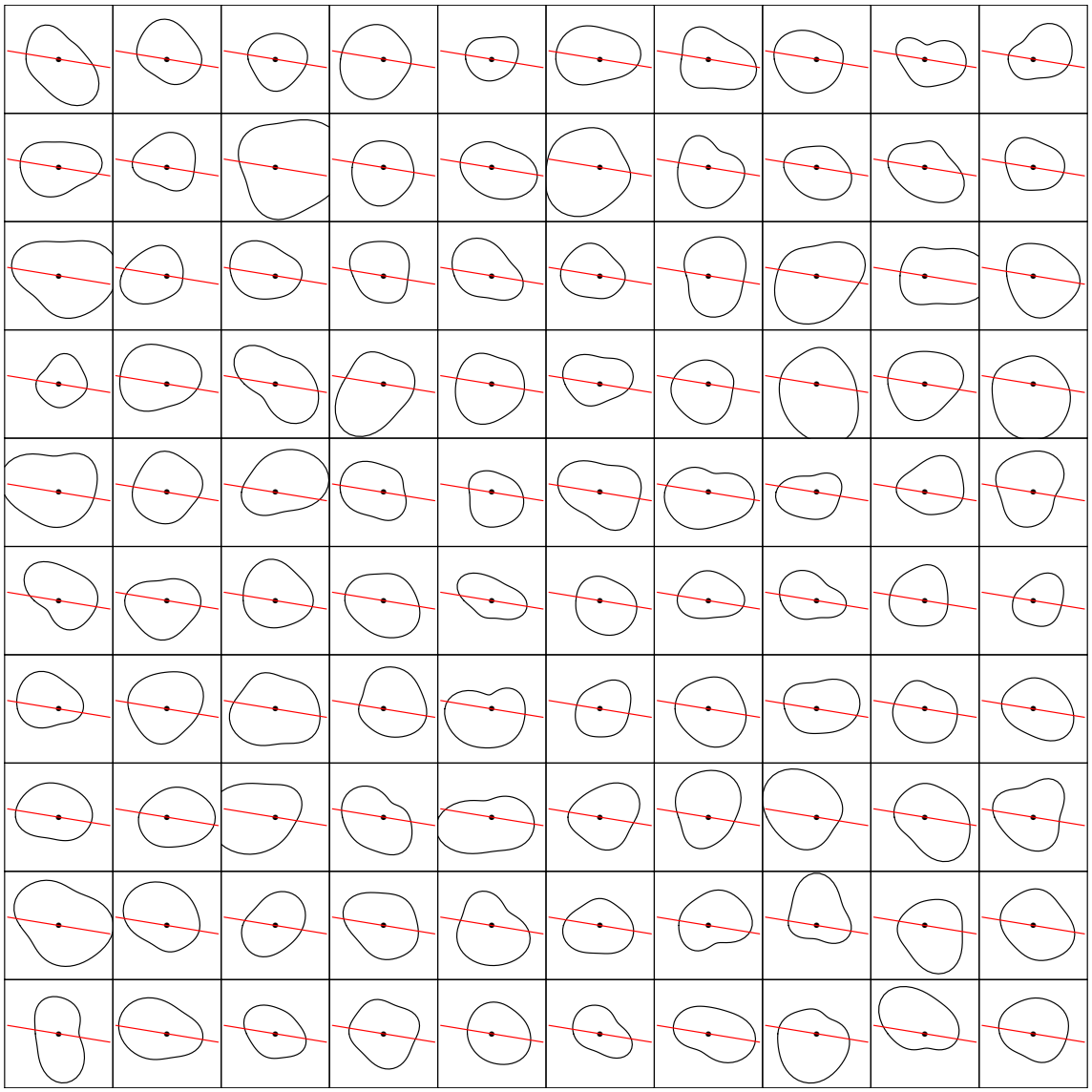

Figure 8: Profiles of 100 particles simulated from the restricted isotropy model as described in the right part of Table 2 in a plane through their reference points perpendicular to $v = (0, 0, 1)^\top$. The direction of the vertical axis u is marked as a line for each particle.

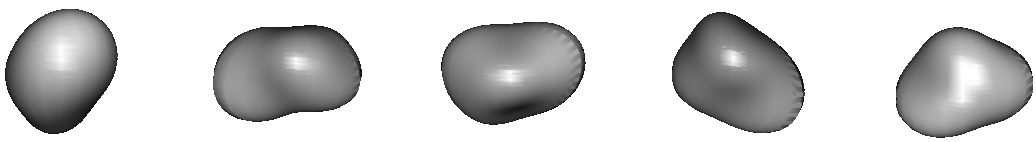

Figure 9: Particles simulated from the fitted model under the assumption of restricted isotropy. The parameter values are given in Table 2.

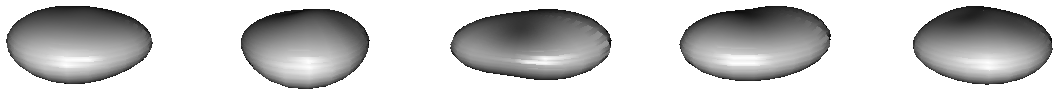

Figure 10: Particles simulated from the model with parameter values given in Table 1.

7 Simulation study

7.1 Statistical performance of the moment estimators

The aim of the simulation study is to investigate the statistical properties of the estimators discussed in Section 4.3 of the mean and covariance matrix of the cover density, as a function of the number n of particles sampled. The stochastic particle model, presented in Section 6, is used in the simulations. We simulated 50,000 particles, each, from the anisotropic model and the restricted isotropy model, whose parameters are given in Tables 1 and 2, respectively. The anisotropic model is much less variable than the restricted isotropy model as can be seen in the illustrations in Figures 9 and 10. The particles were measured using the optical rotator design described in Section 3 and Appendix A.

Using subsamples of sizes $n \in \{25, 100, 200\}$, we analysed the estimators $\widehat{\mu}$ and $\widehat{\Sigma}$. The sample size used for the estimation is denoted by n, and n_{simu} indicates how many samples of size n were analysed. In Tables 3 and 4 the mean and covariance of $\widehat{\mu}$ are given for the two different models, respectively. For each subsample of size n the covariance $\text{cov}(\widehat{\mu})$ was also estimated using the approximation formula (4.5). The mean of these estimates is given in the last column of the tables. Note that the bias of $\widehat{\mu}$ is negligible and the approximation formula (4.5) works well, also for small n.

The mean and componentwise variance of $\widehat{\Sigma}$ can be found in Tables 5 and 6 for the anisotropic and the restricted isotropy model, respectively. The true covariances Σ_{ani} and Σ_{riso} for the anisotropic and the restricted isotropy model, respectively, are given by

$$\Sigma_{\text{ani}} = \begin{pmatrix} 9.479 & -0.575 & -0.031 \\ -0.575 & 11.274 & -0.067 \\ -0.031 & -0.067 & 1.992 \end{pmatrix}, \quad \Sigma_{\text{riso}} = \begin{pmatrix} 9.273 & 0 & -0.421 \\ 0 & 6.702 & 0 \\ -0.421 & 0 & 6.771 \end{pmatrix}. \quad (7.1)$$

The last columns of Tables 5 and 6 contain the mean of the componentwise variances estimated using the approximation formula (4.6). Again, the estimators are well-behaved.

Table 7 summarizes the mean and covariance of the estimated semi-axes of the Miles ellipsoid for both simulated models. Note that the bias of the estimated semi-axes is small, also for $n = 25$.

Table 3: Estimated mean of the cover density for the anisotropic model with parameters given in Table 1. The true mean of the cover density is $\mu = c_0 = (-0.111, -0.224, 0.069)^\top$. The last column gives the mean of the covariance estimated from the subsamples using the approximation formula (4.5).

n	n_{simu}	$\mathbb{E}\widehat{\mu}$	$n\,\text{cov}(\widehat{\mu})$	$n\,\mathbb{E}\widehat{\text{cov}}(\widehat{\mu})$
25	2000	$\begin{pmatrix}-0.106\\-0.212\\0.067\end{pmatrix}$	$\begin{pmatrix}0.622 & 0.331 & 0.01\\0.331 & 2.126 & 0.001\\0.01 & 0.001 & 0.197\end{pmatrix}$	$\begin{pmatrix}0.624 & 0.303 & 0.006\\0.303 & 2.06 & -0.01\\0.006 & -0.01 & 0.201\end{pmatrix}$
100	500	$\begin{pmatrix}-0.106\\-0.213\\0.066\end{pmatrix}$	$\begin{pmatrix}0.612 & 0.353 & 0.009\\0.353 & 2.148 & 0.03\\0.009 & 0.03 & 0.201\end{pmatrix}$	$\begin{pmatrix}0.647 & 0.325 & 0.007\\0.325 & 2.199 & -0.008\\0.007 & -0.008 & 0.202\end{pmatrix}$
200	250	$\begin{pmatrix}-0.106\\-0.214\\0.066\end{pmatrix}$	$\begin{pmatrix}0.576 & 0.308 & 0.016\\0.308 & 2.228 & 0.059\\0.016 & 0.059 & 0.19\end{pmatrix}$	$\begin{pmatrix}0.652 & 0.331 & 0.007\\0.331 & 2.226 & -0.007\\0.007 & -0.007 & 0.202\end{pmatrix}$

Table 4: Estimated mean of the cover density for the restricted isotropy model with parameters given in Table 2. The true mean of the cover density is $\mu = c_0 = (-0.111, -0.224, 0.069)^\top$. The last column gives the mean of the covariance estimated from the subsamples using the approximation formula (4.5).

n	n_{simu}	$\mathbb{E}\widehat{\mu}$	$n\,\text{cov}(\widehat{\mu})$	$n\,\mathbb{E}\widehat{\text{cov}}(\widehat{\mu})$
25	2000	$\begin{pmatrix}-0.118\\-0.224\\0.062\end{pmatrix}$	$\begin{pmatrix}2.277 & 0.025 & 0.019\\0.025 & 2.313 & 0.004\\0.019 & 0.004 & 2.255\end{pmatrix}$	$\begin{pmatrix}2.038 & -0.002 & -0.02\\-0.002 & 2.172 & 0.018\\-0.02 & 0.018 & 2.198\end{pmatrix}$
100	500	$\begin{pmatrix}-0.118\\-0.225\\0.062\end{pmatrix}$	$\begin{pmatrix}2.406 & 0.049 & -0.101\\0.049 & 2.505 & 0.073\\-0.101 & 0.073 & 2.193\end{pmatrix}$	$\begin{pmatrix}2.201 & -0.003 & -0.021\\-0.003 & 2.349 & 0.011\\-0.021 & 0.011 & 2.368\end{pmatrix}$
200	250	$\begin{pmatrix}-0.117\\-0.225\\0.062\end{pmatrix}$	$\begin{pmatrix}2.436 & 0.174 & -0.119\\0.174 & 2.758 & 0.224\\-0.119 & 0.224 & 2.049\end{pmatrix}$	$\begin{pmatrix}2.227 & -0.003 & -0.02\\-0.003 & 2.381 & 0.01\\-0.02 & 0.01 & 2.397\end{pmatrix}$

Table 5: Estimated covariance of the cover density for the anisotropic model with parameters given in Table 1. The true covariance of the cover density is given at (7.1).

n	n_{simu}	$\mathbb{E}\widehat{\Sigma}$	$n\,\text{var}(\widehat{\Sigma})$	$n\,\mathbb{E}\widehat{\text{var}}(\widehat{\Sigma})$
25	2000	$\begin{pmatrix}9.417 & -0.573 & -0.025\\-0.573 & 11.077 & -0.038\\-0.025 & -0.038 & 1.989\end{pmatrix}$	$\begin{pmatrix}7.661 & 15.011 & 1.145\\15.011 & 54.901 & 5.129\\1.145 & 5.129 & 0.792\end{pmatrix}$	$\begin{pmatrix}7.391 & 14.282 & 1.167\\14.282 & 51.122 & 5.148\\1.167 & 5.148 & 0.817\end{pmatrix}$
100	500	$\begin{pmatrix}9.45 & -0.604 & -0.023\\-0.604 & 11.239 & -0.04\\-0.023 & -0.04 & 1.991\end{pmatrix}$	$\begin{pmatrix}7.696 & 14.498 & 1.158\\14.498 & 56.771 & 5.374\\1.158 & 5.374 & 0.761\end{pmatrix}$	$\begin{pmatrix}7.849 & 14.937 & 1.183\\14.937 & 56.625 & 5.171\\1.183 & 5.171 & 0.815\end{pmatrix}$
200	250	$\begin{pmatrix}9.456 & -0.608 & -0.023\\-0.608 & 11.267 & -0.04\\-0.023 & -0.04 & 1.991\end{pmatrix}$	$\begin{pmatrix}7.868 & 15.148 & 1.15\\15.148 & 57.775 & 5.139\\1.15 & 5.139 & 0.806\end{pmatrix}$	$\begin{pmatrix}7.943 & 15.029 & 1.187\\15.029 & 57.672 & 5.183\\1.187 & 5.183 & 0.815\end{pmatrix}$

Table 6: Estimated covariance of the cover density for the restricted isotropy model with parameters given in Table 2. The true covariance of the cover density is given at (7.1).

n	n_{simu}	$\mathbb{E}\widehat{\Sigma}$	$n\,\text{var}(\widehat{\Sigma})$	$n\,\mathbb{E}\widehat{\text{var}}(\widehat{\Sigma})$
25	2000	$\begin{pmatrix} 9.152 & -0.029 & -0.399 \\ -0.029 & 6.559 & 0.008 \\ -0.399 & 0.008 & 6.637 \end{pmatrix}$	$\begin{pmatrix} 32.632 & 15.588 & 16.058 \\ 15.588 & 39.63 & 25.292 \\ 16.058 & 25.292 & 41 \end{pmatrix}$	$\begin{pmatrix} 28.778 & 15.444 & 15.814 \\ 15.444 & 34.137 & 22.733 \\ 15.814 & 22.733 & 34.951 \end{pmatrix}$
100	500	$\begin{pmatrix} 9.268 & -0.027 & -0.399 \\ -0.027 & 6.674 & 0.005 \\ -0.399 & 0.005 & 6.744 \end{pmatrix}$	$\begin{pmatrix} 33.81 & 16.719 & 16.885 \\ 16.719 & 43.244 & 29.013 \\ 16.885 & 29.013 & 45.4 \end{pmatrix}$	$\begin{pmatrix} 35.381 & 15.07 & 15.499 \\ 15.07 & 42.315 & 27.249 \\ 15.499 & 27.249 & 43.548 \end{pmatrix}$
200	250	$\begin{pmatrix} 9.286 & -0.028 & -0.4 \\ -0.028 & 6.694 & 0.003 \\ -0.4 & 0.003 & 6.762 \end{pmatrix}$	$\begin{pmatrix} 32.918 & 16.108 & 15.737 \\ 16.108 & 44.868 & 27.451 \\ 15.737 & 27.451 & 50.225 \end{pmatrix}$	$\begin{pmatrix} 36.572 & 15.008 & 15.417 \\ 15.008 & 43.983 & 28.151 \\ 15.417 & 28.151 & 45.323 \end{pmatrix}$

Table 7: Mean and covariance of the estimated semi-axes of the Miles ellipsoids for the two simulated models. The true parameters are given in Tables 1 and 2.

		Anisotropic model		Restricted isotropy	
n	n_{simu}	$\mathbb{E}(\hat{a}_1,\hat{a}_2,\hat{a}_3)^\top$	$n\,\text{cov}((\hat{a}_1,\hat{a}_2,\hat{a}_3)^\top)$	$\mathbb{E}(\hat{a}_1,\hat{a}_2,\hat{a}_3)^\top$	$n\,\text{cov}((\hat{a}_1,\hat{a}_2,\hat{a}_3)^\top)$
25	2000	$\begin{pmatrix} 7.354 \\ 6.491 \\ 3.029 \end{pmatrix}$	$\begin{pmatrix} 8.102 & 1.933 & -0.269 \\ 1.933 & 1.809 & -0.142 \\ -0.269 & -0.142 & 0.269 \end{pmatrix}$	$\begin{pmatrix} 5.838 \\ 4.983 \\ 4.983 \end{pmatrix}$	$\begin{pmatrix} 2.66 & -0.215 & -0.215 \\ -0.215 & 1.143 & 1.143 \\ -0.215 & 1.143 & 1.143 \end{pmatrix}$
100	500	$\begin{pmatrix} 7.292 \\ 6.544 \\ 3.033 \end{pmatrix}$	$\begin{pmatrix} 10.414 & 1.559 & -0.358 \\ 1.559 & 1.293 & -0.074 \\ -0.358 & -0.074 & 0.255 \end{pmatrix}$	$\begin{pmatrix} 5.832 \\ 4.988 \\ 4.988 \end{pmatrix}$	$\begin{pmatrix} 2.761 & -0.356 & -0.356 \\ -0.356 & 1.262 & 1.262 \\ -0.356 & 1.262 & 1.262 \end{pmatrix}$
200	250	$\begin{pmatrix} 7.288 \\ 6.547 \\ 3.033 \end{pmatrix}$	$\begin{pmatrix} 10.964 & 1.57 & -0.389 \\ 1.57 & 1.367 & -0.06 \\ -0.389 & -0.06 & 0.281 \end{pmatrix}$	$\begin{pmatrix} 5.831 \\ 4.989 \\ 4.989 \end{pmatrix}$	$\begin{pmatrix} 2.913 & -0.491 & -0.491 \\ -0.491 & 1.297 & 1.297 \\ -0.491 & 1.297 & 1.297 \end{pmatrix}$

7.2 Level and power of the isotropy test

In order to assess the level and power of the non-parametric isotropy test, we conducted a simulations study with independent and identically distributed particles following the particle model described in Section 6 for different sets of parameters. We considered two isotropic models and two models that fulfil the assumption of restricted isotropy. Overall, the test is well-behaved for reasonable sample sizes and also shows satisfactory power.

For the isotropic models, $\mathcal{E}$ is a sphere with radius 5.475. For the first model the parameters κ and τ were chosen to induce only moderate variations from a spherical shape, whereas in the second model more variability is observed. In both cases the centre c_0 is slightly moved away from the origin. For the exact parameter values and an illustration of the resulting particles, see Figures 11 and 12 for the first and second isotropy model, respectively.

We simulated $N = 105,000$ particles for each of the two models. For different sample sizes $n \in \{25, 50, 100, 150, 200\}$ we calculated the empirical level of the isotropy test resulting from $n_{\text{simu}} = N/n$ realizations of the test statistic T for desired levels $\alpha \in \{0.01, 0.05, 0.1\}$. The results are summarized in Table 8. The test appears to be slightly conservative for sample sizes $n = 25$, whereas for sample sizes of $n = 50$ or larger the desired level is kept reasonably well.

To investigate the power of the proposed test, we simulated particles from two

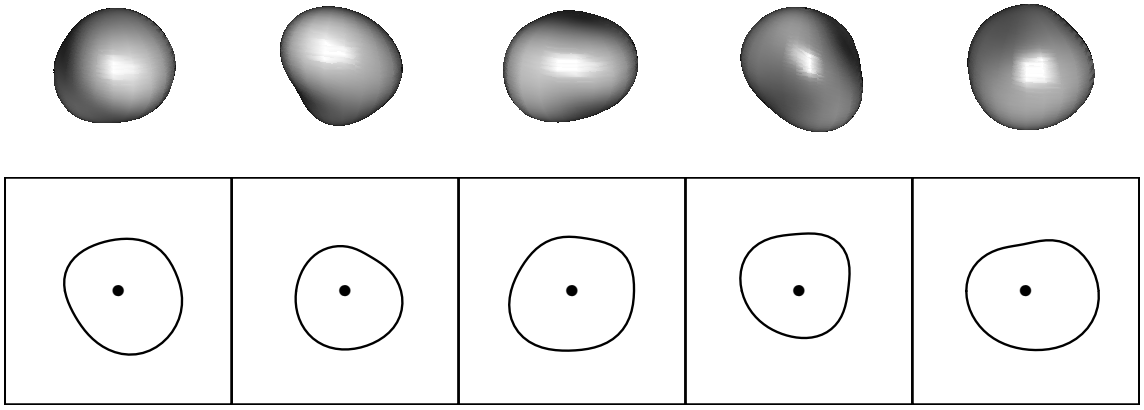

Figure 11: Five particles simulated from the first isotropic model with $a = b = c = 5.475$, $\tau = 1826.117$, $\kappa = 21.106$, $c_0 = (-0.514, -0.417, -0.094)$. In the second row, profiles of the particles in a plane through c_0 perpendicular to $(0, 0, 1)$ are displayed.

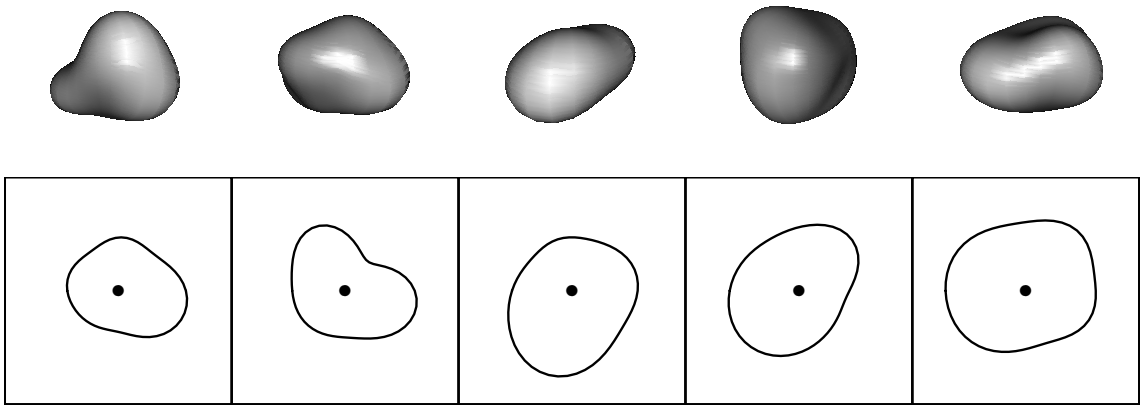

Figure 12: Five particles simulated from the second isotropic model with $a = b = c = 5.475$, $\tau = 471.292$, $\kappa = 5.296$, $c_0 = (-0.514, -0.417, -0.094)$. In the second row, profiles of the particles in a plane through c_0 perpendicular to $(0, 0, 1)$ are displayed.

Table 8: Empirical levels of the isotropy test for the isotropic models described in Figures 11 and 12. The first column gives the sample size n used for the test, n_{simu} refers to the number of realizations of the test statistic used to determine the empirical level for different levels α.

		First model			Second model		
n	n_{simu}	$\alpha = 0.01$	$\alpha = 0.05$	$\alpha = 0.1$	$\alpha = 0.01$	$\alpha = 0.05$	$\alpha = 0.1$
25	4200	0.003	0.042	0.1	0.001	0.026	0.082
50	2100	0.012	0.056	0.112	0.008	0.048	0.109
100	1050	0.012	0.07	0.127	0.012	0.056	0.111
150	700	0.006	0.051	0.106	0.011	0.049	0.104
200	525	0.013	0.067	0.124	0.006	0.044	0.101

anisotropic models that are illustrated in Figures 13 and 14. Both anisotropic models considered fulfil the assumption of restricted isotropy. The first model can be considered to be closer to isotropy than the second model, so we expect a higher power of the test in the second case.

We simulated 96,000 particles from the first model and 56,000 from the second model. The numerical values of the model parameters are given in Figures 13 and 14. The power of the anisotropy test for different levels α is summarized in Table 9. It is clear that a sample size of $n = 25$ is not sufficient to ensure a reasonable power of the test. For a level of $\alpha = 0.05$ the test performs well for sample sizes of at least $n = 100$.

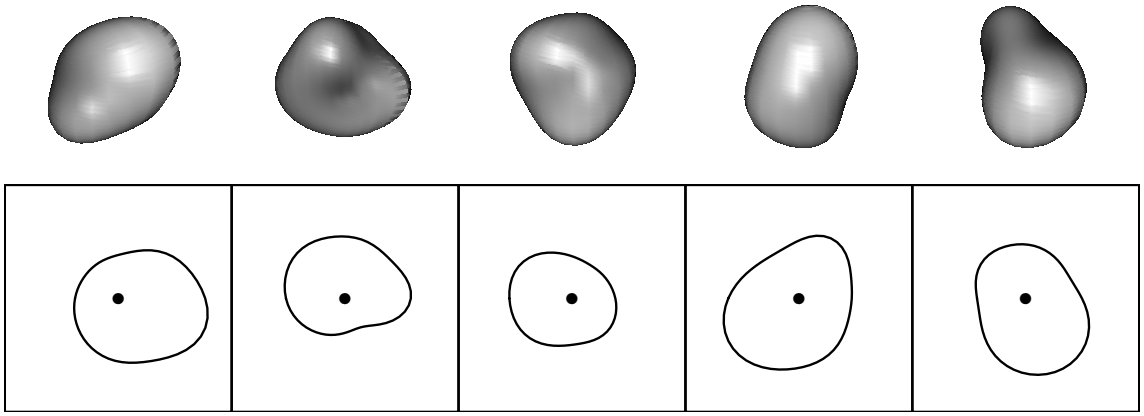

Figure 13: Five particles simulated from the first anisotropic model with $a = 5.841$, $b = c = 5.3$, $\tau = 518.447$, $\kappa = 5.847$, $c_0 = (-0.514, -0.417, -0.094)$. In the second row, profiles of the particles in a plane through c_0 perpendicular to $(0, 0, 1)$ are displayed.

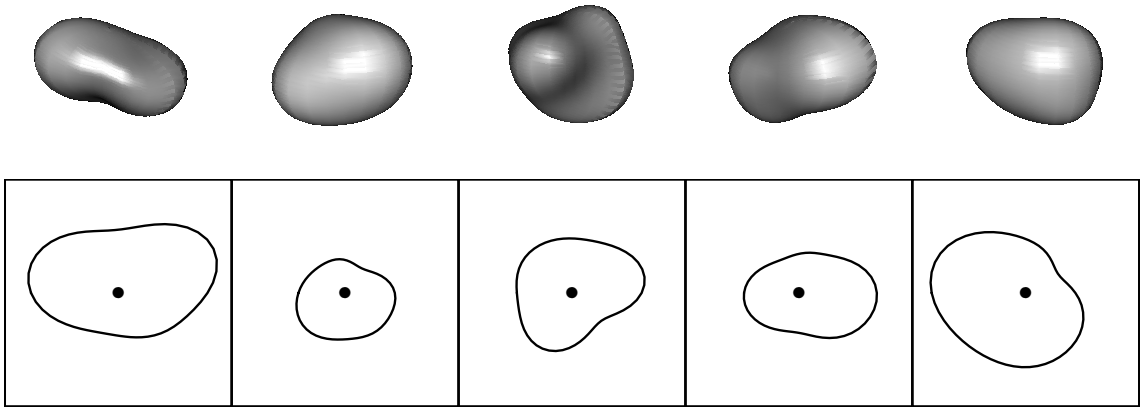

Figure 14: Five particles simulated from the second isotropic model with $a = 6.545$, $b = c = 5.007$, $\tau = 518.447$, $\kappa = 5.847$, $c_0 = (-0.514, -0.417, -0.094)$. In the second row, profiles of the particles in a plane through c_0 perpendicular to $(0, 0, 1)$ are displayed.

Table 9: Empirical powers of the isotropy test for the isotropic models described in Figures 13 and 14. The first column gives the sample size n used for the test, n_{simu} refers to the number of realizations of the test statistic used to determine the empirical power for different levels α.

	First model				Second model			
n	n_{simu}	$\alpha = 0.01$	0.05	0.1	n_{simu}	$\alpha = 0.01$	0.05	0.1
25	3840	0.003	0.048	0.139	2240	0.018	0.252	0.5
50	1920	0.026	0.146	0.262	1120	0.355	0.733	0.871
100	960	0.096	0.293	0.473	560	0.893	0.98	0.998
150	640	0.219	0.489	0.628	373	0.995	0.997	1
200	480	0.365	0.654	0.796	280	1	1	1

Acknowledgements

This research was supported by Centre for Stochastic Geometry and Advanced Bioimaging, funded by the Villum Foundation.

References

I. T. Andersen, J. F. Ziegel, and E. B. Vedel Jensen. Principal roatational formulae. *In preparation*, 2014.

J. Auneau-Cognacq, J. Ziegel, and E. B. Vedel Jensen. Rotational integral geometry of tensor valuations. *Adv. Appl. Math.*, 50:429–444, 2013.

A. Baddeley and E. B. V. Jensen. *Stereology for Statisticians.* Chapman & Hall/CRC, Boca Raton, 2005.

O. E. Barndorff-Nielsen and J. Schmiegel. Lévy based tempo-spatial modeling; with applications to turbulence. *Uspekhi Mat. Nauk*, 159:63–90, 2004.

C. Beisbart, R. Dahlke, K. R. Mecke, and H. Wagner. Vector- and tensor-valued descriptors for spatial patterns. In *Morphology of Condensed Matter*, volume 600 of *Lecture Notes in Physics*, pages 249–271. Springer, Berlin, 2002.

C. Beisbart, M. S. Barbosa, H. Wagner, and L. da F. Costa. Extended morphometric analysis of neuronal cells with Minkowski valuations. *Eur. Phys. J. B*, 52:531–546, 2006.

L. M. Cruz-Orive. Particle size-shape distributions: the general spheroid problem. i. mathematical model. *J. Microsc.*, 107:235–253, 1976.

L. M. Cruz-Orive. Particle size-shape distributions: the general spheroid problem. II. Stochastic model and practical guide. *J. Microsc.*, 112:153–167, 1978.

D. J. Daley and D. Vere-Jones. *An Introduction to the Theory of Point Processes, Volume II: General Theory and Structure.* Springer, New York, 2nd edition, 2008.

E. B. Denis, C. Barat, D. Jeulin, and C. Ducottet. 3D complex shape characterizations by statistical analysis: Application to aluminium alloys. *Mater. Charact.*, 59:338–343, 2008.

M.-L. Hannila, E. B. V. Jensen, A. Hobolth, and J. R. Nyengaard. Shape modelling of spatial particles from planar central sections – a case study. *J. Microsc.*, 215:183–190, 2004.

L. V. Hansen, T. L. Thorarinsdottir, and T. Gneiting. Lévy particles: Modelling and simulating star-shaped random sets. *CSGB Research Report*, 2011. `http://data.imf.au.dk/publications/csgb/2011/imf-csgb-2011-04.pdf`.

G. Hellmund, M. Prokesova, and E. B. Vedel Jensen. Lévy-based Cox point processes. *Adv. Appl. Prob.*, 40:603–629, 2008.

A. Hobolth. The spherical deformation model. *Biostatistics*, 4:583–595, 2003.

E. B. V. Jensen. *Local Stereology.* World Scientific, London, 1998.

E. B. Vedel Jensen. Valuation theory and its applications. Lecture notes, 2011.

E. B. Vedel Jensen and J. F. Ziegel. Local stereology of tensors of convex bodies. *Methodol. Comput. Appl. Probab., to appear*, 2013. doi: 10.1007/s11009-013-9337-8.

K. ÝR Jónsdóttir, J. Schmiegel, and E. B. Vedel Jensen. Lévy-based growth models. *Bernoulli*, 14:62–90, 2008.

R. Schneider and W. Weil. *Stochastic and Integral Geometry.* Springer, Berlin, 2008.

G. E. Schröder-Turk, S. C. Kapfer, B. Breidenbach, C. Beisbart, and K. Mecke. Tensorial Minkowski functionals and anisotropy measures for planar patterns. *J. Microsc.*, 238: 57–74, 2011a.

G. E. Schröder-Turk, W. Mickel, S. C. Kapfer, M. A. Klatt, F. M. Schaller, M. J. F. Hoffmann, N. Kleppmann, P. Armstrong, A. Inayat, D. Hug, M. Reichelsdorfer, W. Peukert, W. Schwieger, and K. Mecke. Minkowski tensor shape analysis of cellular, granular and porous structures. *Adv. Mater.*, 23:2535–2553, 2011b.

T. Tandrup, H. J. G. Gundersen, and E. B. V. Jensen. The optical rotator. *J. Microsc.*, 186:108–120, 1997.

A The optical rotator design

If we observe a vertical random slice $T_2 = L_2 + B(O,t)$ of thickness $2t$ around the axis L_1, then a design-unbiased estimator of $\Phi_r(K)$ is given by

$$\widehat{\Phi}_r(K) = \frac{1}{r!} \int_{K \cap T_2} x^r F_{1,1}\Big(\frac{t^2}{d(x, L_1)^2}\Big)^{-1} \mathrm{d}x,$$

where

$$F_{1,1}(x) = \begin{cases} 0, & \text{if } x < 0 \\ \frac{2}{\pi}\arcsin(\sqrt{x}), & \text{if } 0 \le x \le 1 \\ 1, & \text{if } x > 1 \end{cases}$$

is the distribution function of a beta-distribution with parameters $\alpha = \beta = 1/2$ (Jensen, 1998, Proposition 6.2).

The slice T_2 is now subsampled with a uniformly translated systematic grid of planes parallel to L_2. Each such plane is of the form $L_2 + \delta v$, where $\delta \in [-t, t]$, and v is a unit vector perpendicular to L_2. In such a plane we need to determine

$$\int_{K \cap (L_2 + \delta v)} x^r F_{1,1}\Big(\frac{t^2}{d(x, L_1)^2}\Big)^{-1} \mathrm{d}x.$$

We discretise this integral by a uniformly translated systematic grid of lines in $L_2 + \delta v$. We focus on the case where K intersected with such a line is a line-segment.

First, we treat the case where these lines are parallel to L_1. Let $w \in L_2$ be a unit vector perpendicular to L_1. Then,

$$\int_{K \cap (L_2 + \delta v)} x^r F_{1,1}\Big(\frac{t^2}{d(x, L_1)^2}\Big)^{-1} \mathrm{d}x = \int_{\mathbb{R}} \int_{K \cap (L_1 + \delta v + \tau w)} x^r F_{1,1}\Big(\frac{t^2}{d(x, L_1)^2}\Big)^{-1} \mathrm{d}x \, \mathrm{d}\tau.$$

Let u be a unit vector that spans L_1. For each τ (small enough) there are real numbers $b_- < b_+$ such that $K \cap (L_1 + \delta v + \tau w) = \{\rho u + \delta v + \tau w \mid \rho \in [b_-, b_+]\}$. Then, we obtain

$$\begin{aligned} &\int_{K \cap (L_1 + \delta v + \tau w)} x^r F_{1,1}\Big(\frac{t^2}{d(x, L_1)^2}\Big)^{-1} \mathrm{d}x \\ &\quad = F_{1,1}\Big(\frac{t^2}{\|\delta v + \tau w\|^2}\Big)^{-1} \int_{b_-}^{b_+} (\rho u + \delta v + \tau w)^r \, \mathrm{d}\rho \\ &\quad = F_{1,1}\Big(\frac{t^2}{\delta^2 + \tau^2}\Big)^{-1} \sum_{s=0}^{r} \binom{r}{s} \int_{b_-}^{b_+} \rho^s d\rho \, u^s (\delta v + \tau w)^{r-s} \\ &\quad = F_{1,1}\Big(\frac{t^2}{\delta^2 + \tau^2}\Big)^{-1} \sum_{s=0}^{r} \binom{r}{s} \frac{1}{s+1} (b_+^{s+1} - b_-^{s+1}) u^s (\delta v + \tau w)^{r-s}, \end{aligned}$$

using the binomial formula for symmetric tensors; see e.g., Jensen (2011, Lemma 4.1).

Now, we treat the case where the lines in $L_2 + \delta v$ are perpendicular to L_1. With the notation as above we obtain

$$\int_{K \cap (L_2 + \delta v)} x^r F_{1,1}\Big(\frac{t^2}{d(x, L_1)^2}\Big)^{-1} \mathrm{d}x = \int_{\mathbb{R}} \int_{K \cap (\langle w \rangle + \delta v + \tau u)} x^r F_{1,1}\Big(\frac{t^2}{d(x, L_1)^2}\Big)^{-1} \mathrm{d}x \, \mathrm{d}\tau.$$

For each τ (small enough) there are real numbers $d_- < d_+$ such that $K \cap (\langle w \rangle + \delta v + \tau u) = \{\rho w + \delta v + \tau u \mid \rho \in [d_-, d_+]\}$. Then,

$$\begin{aligned}
&\int_{K\cap(\langle w\rangle+\delta v+\tau u)} x^r F_{1,1}\Big(\frac{t^2}{d(x,L_1)^2}\Big)^{-1}\,\mathrm{d}x \\
&\quad= \int_{d_-}^{d_+} (\rho w+\delta v+\tau u)^r F_{1,1}\Big(\frac{t^2}{d(\rho w+\delta v+\tau u,\langle u\rangle)^2}\Big)^{-1}\,\mathrm{d}\rho \\
&\quad= \int_{d_-}^{d_+} (\rho w+\delta v+\tau u)^r F_{1,1}\Big(\frac{t^2}{\|\rho w+\delta v\|^2}\Big)^{-1}\,\mathrm{d}\rho \\
&\quad= \sum_{s=0}^{r}\binom{r}{s}\int_{d_-}^{d_+} \rho^s F_{1,1}\Big(\frac{t^2}{\rho^2+\delta^2}\Big)^{-1} d\rho\, w^s(\delta v+\tau u)^{r-s}.
\end{aligned}$$

These integrals cannot be integrated explicitly, but numerical integration can be used.

B Moments of the random field ε

In order to calculate the moments of the random field ε, we used the results on the cumulant generating function of Lévy based models that can for example be found in Jónsdóttir et al. (2008).

The cumulant generating function of a gamma random variable Z' with parameters κ and τ is given by

$$C(\lambda \ddagger Z') = -\kappa \log\Big(1-\frac{i\lambda}{\tau}\Big), \quad \lambda \in \mathbb{R}.$$

Therefore, the cumulant generating function of $\varepsilon(u)$ is given by

$$\begin{aligned}
C(\lambda \ddagger \varepsilon(u)) &= \int_{\mathbb{S}^2} C(\lambda k(u,v) \ddagger Z')\mathrm{d}v \\
&= -\kappa \int_{\mathbb{S}^2} \log\Big(1-\frac{i\lambda k(u,v)}{\tau}\Big)\mathrm{d}v \\
&= -2\pi\kappa \int_0^{\pi} \log\Big(1-\frac{i\lambda e^{\alpha\cos\theta}}{\tau}\Big)\sin\theta\mathrm{d}\theta \\
&= \frac{-2\pi\kappa}{\alpha}\int_{-\alpha}^{\alpha} \log\Big(1-\frac{i\lambda e^{u}}{\tau}\Big)\mathrm{d}u.
\end{aligned}$$

For λ small enough we can use the Mercator series to rewrite the integrand, and

obtain

$$\begin{aligned} C(\lambda \ddagger \varepsilon(u)) &= \frac{-2\pi\kappa}{\alpha}\int_{-\alpha}^{\alpha}\log\Big(1-\frac{i\lambda e^u}{\tau}\Big)\mathrm{d}u \\ &= \frac{-2\pi\kappa}{\alpha}\int_{-\alpha}^{\alpha}\sum_{n=1}^{\infty}\frac{(-1)^{n+1}}{n}\Big(-\frac{i\lambda e^u}{\tau}\Big)^n\mathrm{d}u \\ &= \frac{2\pi\kappa}{\alpha}\sum_{n=1}^{\infty}\Big(\frac{i\lambda}{\tau}\Big)^n\frac{1}{n}\int_{-\alpha}^{\alpha}e^{nu}\mathrm{d}u \\ &= \frac{2\pi\kappa}{\alpha}\sum_{n=1}^{\infty}\lambda^n\Big(\frac{i}{\tau}\Big)^n\frac{2}{n^2}\sinh(an). \end{aligned}$$

This implies the following formula for the cumulants k_n

$$k_n = \frac{4\pi\kappa}{\alpha}\frac{(n-1)!\sinh(an)}{n\tau^n}.$$

Via the formula

$$\mu_n = k_n + \sum_{i=1}^{n-1}\binom{n-1}{i-1}k_i\mu_{n-i}$$

all the moments of $\varepsilon(u)$ can be calculated.